ACS APPLIED MATERIALS & INTERFACES

Research Article

www.acsami.org

Anchoring High-Concentration Oxygen Vacancies at Interfaces of CeO_{2-x}/Cu toward Enhanced Activity for Preferential CO Oxidation

Shaoqing Chen, Liping Li, Wanbiao Hu, Xinsong Huang, Qi Li, Yangsen Xu, Ying Zuo, and Guangshe Li*

Key Laboratory of Design and Assembly of Functional Nanostructures, Fujian Institute of Research on the Structure of Matter, Chinese Academy of Sciences, Fuzhou 350002, People's Republic of China

Supporting Information

ABSTRACT: Catalysts are urgently needed to remove the residual CO in hydrogen feeds through selective oxidation for large-scale applications of hydrogen proton exchange membrane fuel cells. We herein propose a new methodology that anchors high concentration oxygen vacancies at interface by designing a CeO_{2-x}/Cu hybrid catalyst with enhanced preferential CO oxidation activity. This hybrid catalyst, with more than 6.1% oxygen vacancies fixed at the favorable interfacial sites, displays nearly 100% CO conversion efficiency in H_2-rich streams over a broad temperature window from 120 to 210 °C, strikingly 5-fold wider than that of conventional CeO_2/Cu (i.e., CeO_2 supported on Cu) catalyst. Moreover, the catalyst exhibits a highest cycling stability ever reported, showing no deterioration after five cycling tests, and a super long-time stability beyond 100 h in the simulated operation environment that involves CO_2 and H_2O. On the basis of an arsenal of characterization techniques, we clearly show that the anchored oxygen vacancies are generated as a consequence of electron donation from metal copper atoms to CeO_2 acceptor and the subsequent reverse spillover of oxygen induced by electron transfer in well controlled nanoheterojunction. The anchored oxygen vacancies play a bridging role in electron capture or transfer and drive molecule oxygen into active oxygen species to interact with the CO molecules adsorbed at interfaces, thus leading to an excellent preferential CO oxidation performance. This study opens a window to design a vast number of high-performance metal-oxide hybrid catalysts via the concept of anchoring oxygen vacancies at interfaces.

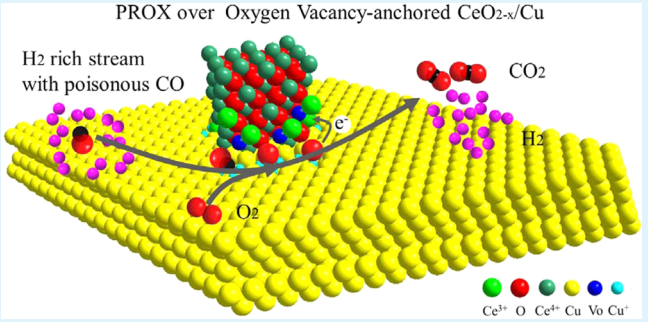

KEYWORDS: *anchoring oxygen vacancies, interface, electron transfer, enhanced activity, preferential CO oxidation, cycling-stability*

1. INTRODUCTION

Hybrid materials based on ceria are massively used in three-way catalytic converters to control automotive exhaust gases (TWC), water−gas shift reaction (WGS), preferential CO oxidation (PROX), fuel cells, catalytic conversion of CO into CO_2 (an important benchmark reaction), and other catalytic applications.[1−4] For all these applications, oxygen vacancies play an important role because the types, concentrations, and distribution of oxygen vacancies dominate the redox properties of ceria-based materials, accounting for the final performance of catalysts.[5−9] In model catalysis, recent experimental and theoretical advances on the catalytic mechanism have revealed that the main reactions occur near the interface of hybrid catalysts and involve oxygen vacancies at interface.[10−12] For example, Liu et al. conclude that the active sites of Au/CeO_2 catalysts for WGS are neither single Au atoms nor sizable Au particles, but $Au^{\delta+}$ in the vicinity of interfacial oxygen vacancies.[13] Moreover, the physical properties and chemical reactivity of inorganic compounds, such as electron transfer, are most associated with the distribution of oxygen vacancies, and the propagation of oxygen vacancies to noninterfacial area may lead to an irreversible deactivation of catalysts.[14−16] As model catalysts, CeO_x/metal with high-concentration oxygen defects were achieved by exposing the supported Ce atoms to O_2, which were vapor deposited on a gold or copper substrate in ultrahigh-vacuum (UHV) chambers.[10,11] Despite of these, it is still challenging to fix high-concentration oxygen vacancies at interfaces of nano heterostructure by a facile chemical process so far, which requires the understanding of the generation machanism of interfacial defects and also call for a feasible method to synthesize high-efficiency catalysts for industrial applications.

Preferential CO oxidation in hydrogen feeds (PROX) is a key reaction for practical implementation of hydrogen proton exchange membrane fuel cells (PEMFC).[15,17−21] Currently, nearly 95% of the world's H_2 supply is accomplished by reforming of hydrocarbons followed by WGS processes.[22−26] This "reformate" H_2 inevitably contains approximately 0.5−1.0 vol % CO, which is thermodynamically favorable at low temperature WGS.[27] Although seemingly very tiny, such an amount of CO would seriously poison the anode of PEMFCs. To reduce the poisonous CO to a trace level below 10 ppm,

Received: July 13, 2015
Accepted: September 29, 2015
Published: October 7, 2015

DOI: 10.1021/acsami.5b06302
ACS Appl. Mater. Interfaces 2015, 7, 22999−23007

Scheme 1. Preparation Scheme of CeO_{2-x}/Cu Catalyst by a Two-Step Precipitation in One-Pot and Two-Step Annealing Processes

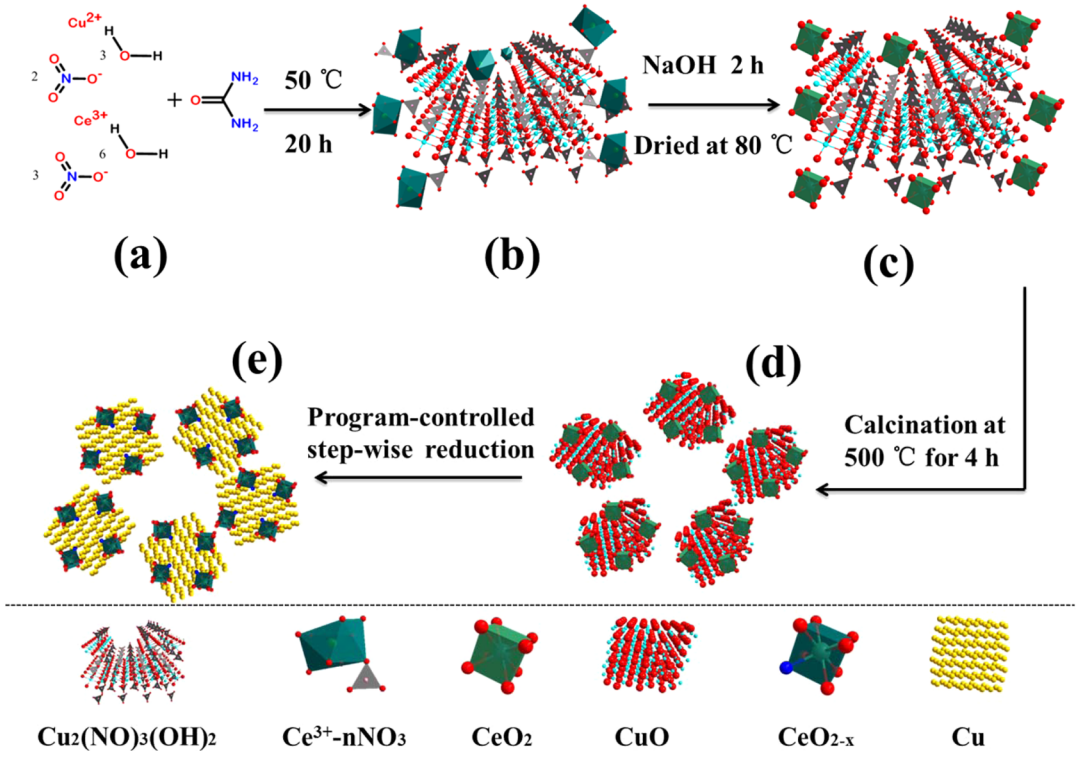

[a]Starting materials. [b]Ce^{3+} absorbed onto $Cu_2(NO_3)(OH)_3$. [c]$CeO_2/Cu_2(NO_3)(OH)_3$. [d]CeO_2/CuO intermediate. [e]V_O-anchored CeO_{2-x}/Cu catalyst.

proper catalysts enabling PROX in hydrogen rich streams are urgently needed.[15,18,28]

The difficulty of achieving this goal is how to obtain a good cycling stability in a wider high temperature range (e.g., 120−200 °C), which offers cost and energy savings, because the down-streams from WGS reactor for excess H_2 is about 200 °C.[17] Among the catalysts that are informed to be active for PROX, copper−ceria-based catalysts have long-term been considered as the attractive candidates because they have get rid of using noble metals. CuO/CeO_2 catalysts (copper oxide patches dispersed onto ceria) and $Cu_xCe_{1-x}O_2$ (copper-doped ceria) catalysts present a poor activity.[29,30] Optimum catalytic properties for preferential CO oxidation were realized over Cu/CeO_2 catalysts with tailored mesostructure and CeO_2-supported Cu-cluster catalysts, which could operate at low temperature range around 80 °C.[31−33] Design of an inverse CeO_2/CuO catalyst and incorporation of promoters such as ZnO, ZrO_2, TiO_2, Fe_2O_3, carbon nanotubes for CuO−CeO_2, have been shown capable of broadening the work temperature windows.[15,34−38] Unfortunately, the catalysts used ever before or currently or is considered to be used all seriously lose CO−PROX activity at temperature above 150 °C, owing to the apparently promoted H_2 oxidation by the propagation of oxygen vacancies to noninterfacial area.[15,30] Further ambiguousness for these catalysts is the underlying mechanism. For instance, for CeO_2 and CuO components, no definite conclusions could be reached because both are active for CO and H_2 oxidation at redox cycles Ce^{4+}/Ce^{3+} and Cu^{2+}/Cu^{+}.

In this work, we report on a new chemical methodology through anchoring oxygen vacancies (V_O) at interface by electron transfer of metal → oxide. This strategy is based on the following considerations: (1) When contacting reducible oxides, metal (M) atoms, especially for d^{10} configuration could donate an electron to form M^+ ions, which is generally considered to be the adsorption sites of CO;[10,39,40] (2) oxygen reverse spillover induced by electron transfer from metal atoms to reducible oxides could produce oxygen vacancies at interfaces, favoring the continuous catalysis;[41,42] and (3) the intrinsically interfacial oxygen vacancies could play a bridging role in electron capture or tranfer to drive molecule oxygen into active oxygen species.[17] We accordingly designed the V_O-anchored CeO_{2-x}/Cu hybrid catalyst by a two-step precipitation and a subsequent two-step annealing processes. Much superior to the conventional catalysts (e.g., CeO_2/CuO and Cu−CeO_2), current CeO_{2-x}/Cu hybrid catalyst greatly broadens the operation temperature window (120−210 °C) with a very high CO convention and excellent cycling stability. The catalyst exhibits a super long-time stability also in the simulated operation environment that contains H_2O and CO_2 in H_2-rich streams, which lasted for a period beyond 100 h with a 100% CO conversion at 150 °C. Furthermore, due to a large family of metal-oxides as candidates, the methodology reported here shows a huge potential to synthesize high-performance composite catalysts with high-concentration oxygen vacancies anchoring at interface for catalytic applications.

2. EXPERIMENTAL SECTION

2.1. Sample Syntheses. *2.1.1. Synthesis of Oxygen Vacancies Anchored CeO_{2-x}/Cu Catalysts.* Oxygen vacancies anchored catalyst (denoted as CeO_{2-x}/Cu) was purposefully synthesized through a multistep process that includes a two-step precipitation in one-pot and subsequently a two-step annealing, as illustrated in Scheme 1 and also described in Supporting Information. Copper(II) and cerium(III)

DOI: 10.1021/acsami.5b06302
ACS Appl. Mater. Interfaces 2015, 7, 22999−23007

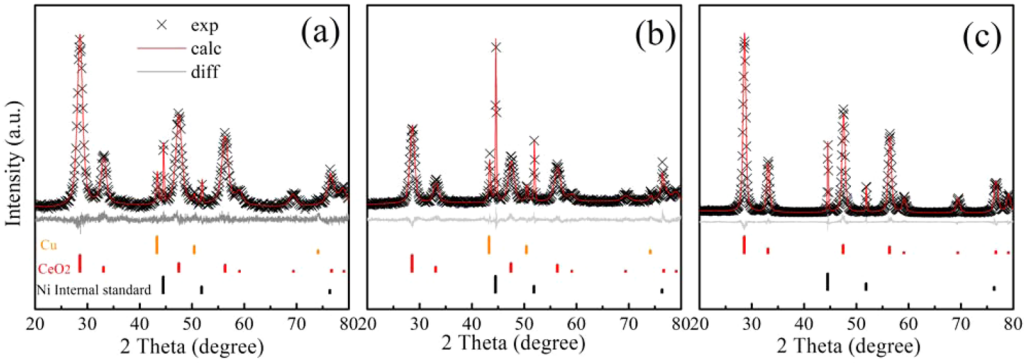

Figure 1. XRD patterns and the data refinements for the samples: (a) V_O-anchored CeO_{2-x}/Cu catalyst; (b) CeO_2/Cu reference and (c) pure CeO_2. All diffraction peaks are well compatible with the standard diffraction data for fluorite CeO_2 (PDF #65-5923) and metallic Cu (PDF #04-0836).

nitrates were chosen as the starting materials, urea as the only additive and NaOH as the precipitation agent. When $Cu(NO_3)_2{\cdot}3H_2O$ and $Ce(NO_3)_3{\cdot}6H_2O$ were dissolved in water that contains urea, a weak acidic condition formed, and $[Cu_2(OH)_2]^{2+}$, the hydrolysis product of Cu^{2+} ions, combined with NO_3^- to form polynuclear complexes of $[Cu_2(OH)_2NO_3]^+$. During the long time stirring at 50 °C, urea slowly hydrolyzed to release OH^- anions that would combine with copper polynuclear complexes, generating the first main precipitant suspension in terms of $Cu_2(NO_3)(OH)_3$ (Scheme 1b and Figures S1 and S2).[43,44] The layered-structure $Cu_2(NO_3)(OH)_3$ could act as the absorbing sites of Ce^{3+} ions. Namely, after first-step precipitation, a lot of Ce^{3+} ions would gather together around the surfaces of $Cu_2(NO_3)(OH)_3$. To precipitate these Ce^{3+} ions, neutral or alkaline conditions are required.[45] The second-step precipitation begins as a certain amount of NaOH is added into the above suspension solution. Once the solution reached a pH > 7, a quick nucleation of ceria species would happen and give rise to CeO_2 nanocrystals of only 4.4 nm in dimension (Scheme 1c and Figure S1) with the assistance of $Cu_2(NO_3)(OH)_3$. With the above two-step precipitations, the precursor $CeO_2/Cu_2(NO_3)(OH)_3$ could be obtained with CeO_2 nanoparticles embedding in large supports. The subsequent two-step annealing allows the formation of final V_O-anchored CeO_{2-x}/Cu: the obtained precursor is first annealed at 500 °C for 4 h in air to form intermediate composite CeO_2/CuO (Scheme 1d and Figure S3). This intermediate composite is then reduced and converted into CeO_{2-x}/Cu catalyst (Scheme 1e, Figures 1a and S3) in a flowing mixed gas containing 50% H_2 as the temperature increases from 60 to 240 °C by a program-controlled stepwise sequence (Figure S9).[46]

2.1.2. Syntheses of Pure CeO_2 and Cu. For the purpose of comparison, we also prepared pure CeO_2 and metallic copper following the above procedure but with minor modifications: For the case of CeO_2, no copper species was involved. For the synthesis of metallic copper, no cerium species was contained.

2.1.3. Synthesis of Classic Inverse Catalyst CeO_2/CuO. The composite classic inverse catalyst CeO_2/CuO was prepared using a reverse microemulsion method, as described in a previous report.[15] Briefly, $Cu(NO_3)_2$ aqueous solution was added into an organnic solution that contains *n*-Heptane, Triton-X-100 and *n*-Hexanol to form a reverse microemulsion. Another reverse microemulsion that contains aqueous solution of tetramethylammonium hydroxide (TMAH) was prepared. TMAH-containing emulsion was added into Cu-containing one to complete the precipitation reactions. After separating and calcining, CuO nanoparticles were achived. Then the powders were dispersed in a similar reverse microemulsion that contains $Ce(NO_3)_3$, and TMAH-containing emulsion was added to precipitate cerium. The resulting deposits were separated and calcined at 500 °C for 3h to get CeO_2/CuO catalysts.

2.1.4. Synthesis of CeO_2/Cu Reference (CeO_2 Supported on Cu). To obtain CeO_2/Cu reference, we further reduced the classic inverse catalyst CeO_2/CuO following the same program-controlled stepwise sequence as mentioned above.

2.2. Characterizations Methods. Crystalline phases of the synthesized materials were identified by an X-ray diffraction (XRD) on a Rigaku DESKTOP, equipped with a Cu Kα radiation source (λ = 1.5418 Å). Cell parameters of the samples were calculated through structural refinements on GASA program using Ni as the internal standard.

Transmission electron microscopy (TEM) and high-resolution TEM (HRTEM) images were obtained on a Tecnai G2 F20 field-emission transmission electron microscope operating at an acceleration voltage of 200 kV.

X-ray photoelectron spectroscopy (XPS) was performed using an ESCA-LAB MKII photoelectron spectrometer equipped with a monochromatic Al Kα ($h\nu$ = 1486.6 eV) radiation source. The charging shift was calibrated using C 1s value of adventitious carbon at binding energy of 284.8 eV. Smart background correction was used for peak fits with Avantage program.

BET surface area and pore volume of the sample were measured by N_2 adsorption−desorption isotherms at −196 °C using Micrometrics ASAP 2020 instrument.

Diffuse reflectance Fourier transform infrared spectroscopy (DRIFTS) of the samples was carried out using CO as probe molecule at room temperature. Prior to measurements, the samples were pretreated in situ with H_2 at 220 °C for 60 min, then Ar at 150 °C for 30 min and cold down to room temperature in an Ar flow.

H_2-TPR tests were carried out at a heating rate of 5 °C min^{-1} using 10 vol % H_2 in Ar and at a flow rate of 20 mL·min^{-1} to examine the redox behaviors of the samples. Note that for CeO_{2-x}/Cu catalyst and CeO_2/Cu reference, 30 mg of the samples were first pretreated in 10 vol % H_2 in Ar in a temperature range from 60 to 300 °C. After cooling down to room temperature in the mixture, the samples were treated in Ar at 120 °C for 2 h. Then, H_2-TPR test starts.

2.3. Catalytic Activity Study. Catalytic activity of the as-prepared catalysts was measured in a feed reactor. The feed contained 1% CO, 1.25% O_2, 50% H_2, and the balance He at a rate of 1×10^3 cm^3 min^{-1} g^{-1} (roughly 80000 h^{-1} GHSV). The cycling stability was tested in a temperature range of 60−240 °C for five cycles. To study the influence of H_2O and CO_2 on catalytic performance, 10% H_2O and 15% CO_2 were added to the H_2-rich feed, respectively. Long-time stability was also tested at a condition that simulates the practical applications, which involves H_2O and CO_2 together in H_2-rich feed at 150 °C. The products and reactants were analyzed by a gas chromatograph equipped with TC-detector. No products other than those resulted from CO or H_2 (i.e., CO_2 and H_2O) were observed under the applied reaction conditions. Basically, the percentage of conversion and selectivity in the CO-PROX process are defined as

$$X_{O_2}(\%) = \frac{F_{O_2}^{in} - F_{O_2}^{out}}{F_{O_2}^{in}} \times 100$$

$$X_{CO}(\%) = \frac{F_{CO}^{in} - F_{CO}^{out}}{F_{CO}^{in}} \times 100$$

DOI: 10.1021/acsami.5b06302
ACS Appl. Mater. Interfaces 2015, 7, 22999−23007

$$S_{CO_2}(\%) = \frac{X_{CO}}{2.5X_{O_2}} \times 100$$

where X and S represent percentage conversion and selectivity, respectively. F is the molar flow of the indicated gas (inlet or outlet).

3. RESULTS AND DISCUSSION

The crystalline structures of final product CeO_{2-x}/Cu, CeO_2/Cu, and pure CeO_2 were examined by XRD. All diffraction peaks are well-defined and match well the standard diffraction data for fluorite CeO_2 and metallic Cu, respectively (Figure 1). As estimated by Scherrer formula, the average crystal sizes are about 6−7 nm for the supported ceria in the present CeO_{2-x}/Cu and CeO_2/Cu reference. The cell a-axis length of the component CeO_{2-x} revealed by XRD date refinement is 5.4330(2) Å, abnormally larger than that of 5.4155(8) Å for CeO_2/Cu sample and 5.4144(1) Å for pure CeO_2 (Figure 1, Table 1). This result indicates the presence of larger-radius of

Table 1. Structural Refinement Results for CeO_{2-x}/Cu, CeO_2/Cu Reference and Pure CeO_2 Using GSAS Software

	cell parameters of fluorite phase				
samples	a (Å)	cell volume (Å^3)	R_p	R_{wp}	X^2
CeO_{2-x}/Cu	5.4330 (2)	160.43(2)	0.0418	0.0527	1.181
CeO_2/Cu reference	5.4155(8)	158.83(1)	0.0489	0.0610	1.675
Pure CeO_2	5.4144 (1)	158.73(1)	0.0559	0.0768	1.489

Ce^{3+} ions (ionic radius 1.143 Å) at the sites of Ce^{4+} ions (0.907 Å). That is, oxygen vacancies must be introduced meanwhile to compensate the charge balance in the as-prepared CeO_{2-x}/Cu catalyst, as reported elsewhere.[15,47]

Microstructural characteristics of CeO_{2-x}/Cu catalyst were investigated by transmission electron microscopy (TEM). As shown in Figure 2a, on the large substrates, there distributes quite a lot of pillar-shaped nanoparticles with a diameter less than 10 nm, which are fluorite-type CeO_2 as confirmed by selective area (magenta square, Figure 2a) high-resolution TEM (HRTEM) image (Figure 2b). Metallic copper was also observed with a lattice spacing of 2.08 Å that corresponds well to the (111) plane of cubic copper. It is quite striking that the interface between nanopillars and substrate could be a heterostructure interface, as shown by a typical HRTEM image (red square, Figure 2a) in Figure 2c. Obviously, the nanopillars should embed in the large substrate Cu with the emergence of an irregular borderline in disordered region. With respect to the heterostructure interface, its width coming from structural disorder was estimated to be about 1.5−2.5 nm. The noninterfacial part of nanopillars shows the lattice spacing of 3.14 Å, and 2.72 Å with an angle of 54.7°, which correspond well to the (111) and (200) planes of CeO_2, respectively. To further make clear the microstructural differences, a detailed comparison was done between interface area (I) and noninterface area (II) as shown in Figure 2d,e. The related structure models were proposed accordingly. In the face-centered cubic (fcc) CeO_2, (200) plane is a pure cerium plane, while the plane between two adjacent (200) planes can be contributed by a layer of O anions, i.e. (400) plane. As clearly see in Figure 2d, the intensity of lattice-fringe image in the interface region decreases significantly along the plane (400) (red line) and moreover, several areas (dark pits in red ellipses)

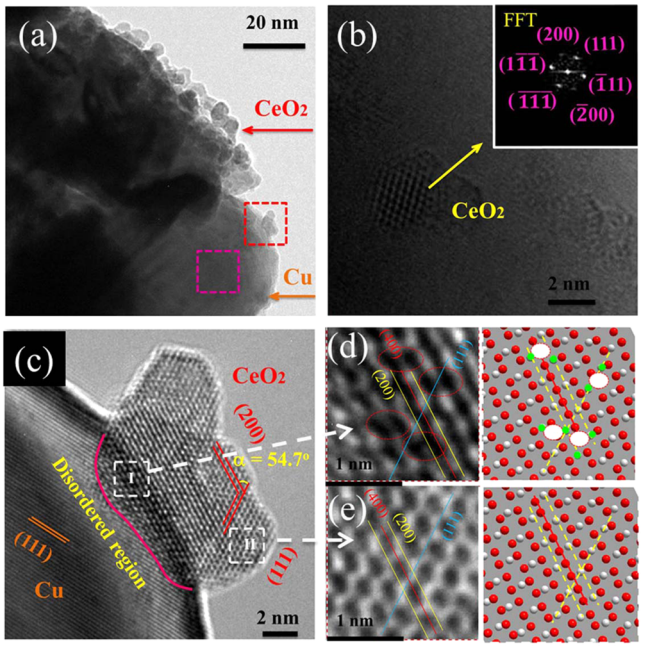

Figure 2. Structural characteristics of CeO_{2-x}/Cu catalyst: (a) TEM image; (b) HRTEM image of a selected area (magenta square in panel a); and (c) HRTEM image for a typical interface (red square in a). A curve is applied to outline the disordered region at interface. (d and e) Enlarged images of the special areas I and II (white squares in panel c), along with the corresponding models (Ce^{4+}, gray ball; Ce^{3+}, green ball; O^{2-}, red ball; defect, white ellipse with red edge). Dark pits (red ellipses in panel d) are highlighted to note the defects of oxygen vacancies.

show the quite different contrast that should be related to the defects (e.g., substitutional Ce^{3+} cations and oxygen vacancies). This sharply compares to the noninterface region where only intact honeycomb-type structures were observed (Figure 2e). Therefore, a substantial conclusion can be drawn: oxygen vacancies were anchored at the interfacial sites of the hybrid catalyst CeO_{2-x}/Cu catalyst, as reported in other systems.[6,48]

Raman spectra were further carried out to characterize the nature of oxygen vacancies in CeO_{2-x}/Cu catalyst. As shown in Figure 3, when compared to pure CeO_2 with the F_{2g} symmetric stretching of Ce−O bond near 460 cm^{-1}, a large Raman downshift was observed for CeO_{2-x}/Cu catalyst with this peak at 446 cm^{-1}. This red shift is most likely due to the lattice expansion and mode softening as induced by oxygen vacancy

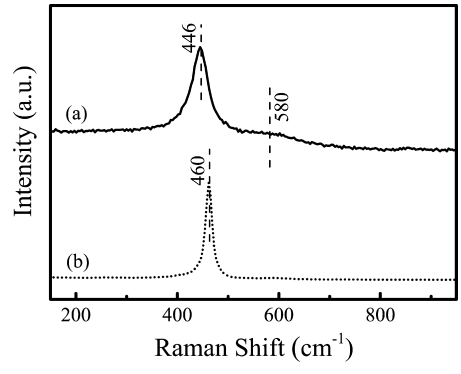

Figure 3. Raman spectra of (a) CeO_{2-x}/Cu catalyst and (b) pure CeO_2 recorded using 532 nm excitation.

DOI: 10.1021/acsami.5b06302
ACS Appl. Mater. Interfaces 2015, 7, 22999−23007

generation, because two Ce^{3+} ions (1.143 Å) have to be replaced by two Ce^{4+} ions (0.907 Å) to maintain the electrostatic balance for each oxygen vacancy when generated.[49] In addition to the strong phonon mode at 446 cm^{-1} from *F2g* symmetric stretching of Ce−O bond, a signal related to oxygen vacancy was observed at 580 cm^{-1}, as reported elsewhere.[31] The wavenumber difference between *F2g* mode and oxygen vacancy signal was 134 cm^{-1}, indicating that oxygen vacancy in CeO_{2-x}/Cu catalyst are from intrinsic defects (i.e., the redox couple of Ce^{4+}−Ce^{3+}).

X-ray photoelectron spectrum of Ce 3d usually exhibits rather complex features due to the hybridization with ligand orbitals and fractional occupancy of the valence 4f orbitals. Previous research has demonstrated that Ce 3d core level of Ce^{4+} containing compounds consists of six photoelectron peaks, while that of Ce^{3+} containing compounds can be resolved in four peaks.[50] Moreover, the peaks at ca. 882 and 916 eV are usually considered as the fingerprints of Ce^{4+} ions, while those at ca. 885 and 903 eV are characteristic of Ce^{3+} ions. Thus, XPS spectrum is a well-established technique to determine the concentration of Ce^{3+} ions through semi-quantitative calculation of the integrated peak area.[50] Figure 4

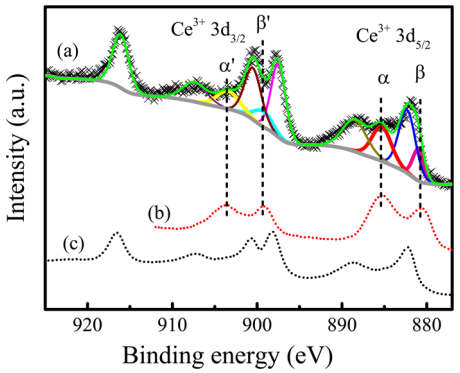

Figure 4. Ce 3d XPS spectra of (a) CeO_{2-x}/Cu and standard XPS data for (b) Ce_2O_3 and (c) CeO_2.

exhibits the Ce 3d core level XPS spectrum of the catalyst. XPS data of Ce_2O_3 and CeO_2 from literature were also given for comparison.[51] Apart from three pairs of characteristic peaks for Ce^{4+}, four obvious peaks (denoted as α, α', β, and β') were also identified and assigned to Ce^{3+} for the CeO_{2-x}/Cu catalyst. The peaks positions and integrate area were listed in Table S1, respectively. The Ce^{3+} concentration can be calculated as follows.[9,50,52]

$$[Ce^{3+}] = A(Ce^{3+})/A(Ce^{3+} + Ce^{4+}) = 24.4\%$$

Then, the corresponding concentration of oxygen vacancy can be calculated as

$$[V_O] = 1 - (3[Ce^{3+}] + 4[Ce^{4+}])/4 = 6.1\%$$

It is worth noting that the concentration of oxygen vacancy at interface is more than 6.1%, owing to the enrichment effect.

It is well-known that pure CeO_2 would be subject to an obvious reduction at high temperature such as 500 °C. How can Ce^{3+}−V_O defects be generated in the present CeO_{2-x}/Cu at such a low temperature? It is still a mystery.[31] To uncover this, we performed diffuse reflectance Fourier transform infrared spectroscopy (DRIFTS) characterization using CO as the probe molecules (Figures 5).[15,53] The relevant data for a

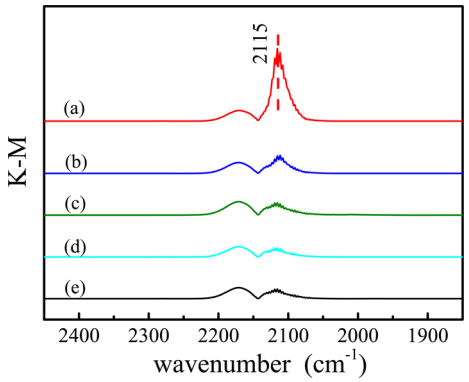

Figure 5. Diffuse reflectance Fourier transform infrared spectra of CO adsorption on the samples: (a) V_O-anchored CeO_{2-x}/Cu catalyst, (b) CeO_2/Cu reference, (c) CeO_2, (d) Cu, and (e) background KBr.

series of reference samples like CeO_2/Cu reference, pure CeO_2, metallic Cu and blank sample (KBr sample) were also involved for comparison. Blank runs were done with KBr sample to distinguish the contributions from the gas phase CO signal. It is clearly seen that CeO_{2-x}/Cu catalyst exhibits a peak at ca. 2115 cm^{-1} with intensity much stronger in magnitude than those of the reference samples of pure CeO_2, metallic Cu and CeO_2/Cu. For the latter cases, its magnitude is only comparable to that of the background KBr. This characteristic peak is attributed to Cu^+−CO that obviously appears only in the presence of CeO_{2-x}/Cu catalyst. Since an in situ pretreatment was done under reduction atmosphere, the production of Cu^+ is concluded to be due to Cu^0 atoms that donate electrons to the adjacent CeO_2, beneficial from the closely contacted CeO_2 of the "embedded in" structure. After capturing electrons, the nearest Ce^{4+} ions are reduced to Ce^{3+}, which could weaken the interface Ce−O bonds and facilitate the generation of more reducible oxygen, giving rise to a high-concentration Ce^{3+}−V_O at interfaces under reduction conditions.[39,54,55]

Reduction ability is one of the most important natures for a catalyst. Temperature-programmed reduction by H_2 (H_2-TPR) was carried out to investigate the reducibility of intermediate CeO_2/CuO product and reference samples, as shown in Figure 6a. For CeO_2/CuO intermediate, the signals (α, β) in the range from 100 to 200 °C are associated with the release of surface and bulk oxygen from CuO, as well as the interface oxygen of CeO_2 activated by metallic copper. Obviously, the reduction peaks shifted to lower temperature by about 150 °C compared to those for classic CeO_2/CuO and pure CuO. The shifts toward lower temperature for reduction peaks were induced by a strong synergistic interaction between the closely contacted CuO and CeO_2, which facilitates the reduction of both component oxides, as reported elsewhere.[31,56]

For the present CeO_{2-x}/Cu catalyst, its reduction ability was comparatively studied in terms of H_2-TPR with a reference of CeO_2/Cu (Figure 6b). Apparently, CeO_{2-x}/Cu catalyst exhibits reduction ability superior to that of CeO_2/Cu reference, because H_2 consumption for the former one is nearly 3 times larger than that for the latter in the temperature range of 100−200 °C. Generally, the reduction in this temperature range is rightly dominated by the active oxygen species at interface.[31] In the present CeO_{2-x}/Cu catalyst, the structure of "CeO_2 embedded in Cu support" weakens the interfacial Ce−O bonds and facilitates the formation of more active oxygen species, that is, nearly 3-fold compared to that in CeO_2/Cu

DOI: 10.1021/acsami.5b06302
ACS Appl. Mater. Interfaces 2015, 7, 22999−23007

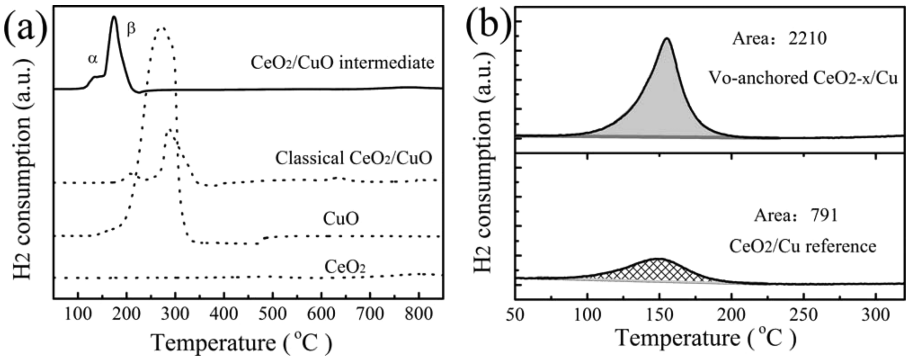

Figure 6. H_2-TPR profiles of the samples: (a) CeO_2/CuO intermediate, the classic CeO_2/CuO composite, pure CuO and CeO_2; and (b) CeO_{2-x}/Cu catalyst and CeO_2/Cu reference.

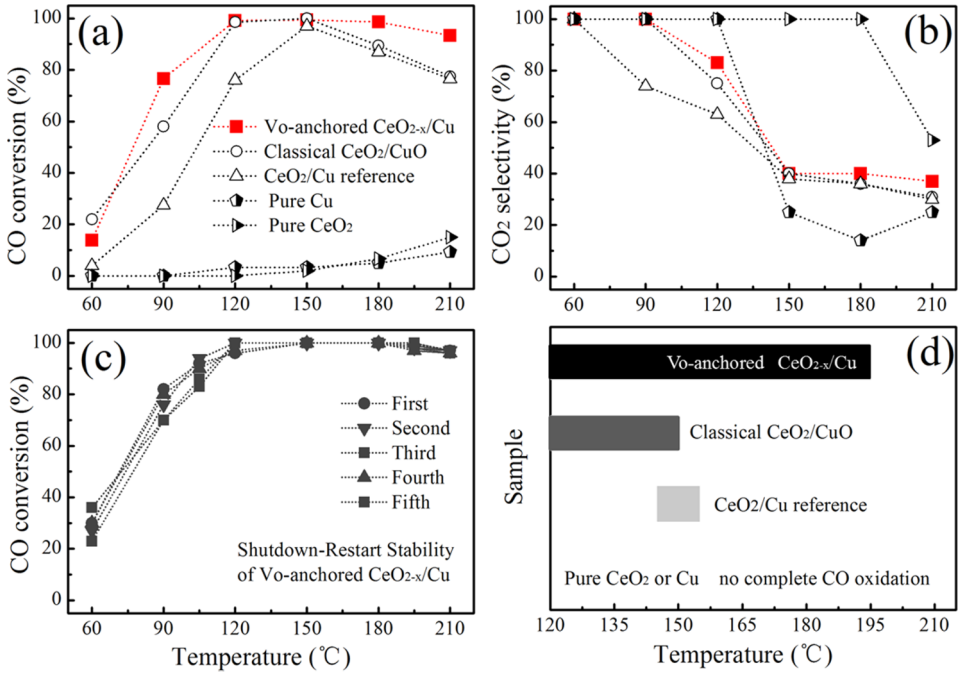

Figure 7. Catalytic performances of the indicated samples under 1% CO, 1.25% O_2, 50% H_2 (He balance): (a) CO conversion; (b) selectivity to CO_2; (c) stability of CeO_{2-x}/Cu catalyst at shutdown-restart cycles; and (d) temperature windows of removing CO to acceptable concentration.

reference, which could be favorable for generating high-concentrate oxygen vacancies.[57]

To conform the superior reduction ability, we investigated the excellent catalytic performance of the present CeO_{2-x}/Cu catalyst in terms of CO-PROX, as shown in Figure 7. Compared to other reference samples like CeO_2/CuO, CeO_2/Cu, CeO_2, or Cu, the current catalyst CeO_{2-x}/Cu shows not only the highest CO conversion efficiency over a broad temperature range (e.g., 90−210 °C) but also the best temperature stability (i.e., the least fluctuations in CO conversion efficiency with temperature variations), strikingly showing an efficiency nearly 100% at temperatures between 120 and 210 °C. By contrast, pure CeO_2 or Cu gives an efficiency <20%. Although CeO_2/CuO or CeO_2/Cu can reach somewhat comparable CO conversion efficiency to CeO_{2-x}/Cu catalyst in a very narrow temperature window (i.e., 120−150 °C), their CO conversion efficiency decreases significantly beyond this temperature window (e.g., only 30−58% at 90 °C, 90% at 180 °C, and 78% at 210 °C; Figure 7a). Due to the competitive oxidation of H_2, the selectivity toward CO_2 for all compound samples decreased gradually in the temperature range from 90 to 150 °C (Figure 7b). It is worth noting that the onset temperature of H_2 oxidation was in accordance with the reduction peaks of interfacial oxygen species (Figure 6b), indicating the occurrence of H_2 oxidation at interfacial sites also. This phenomennon suggests that there maybe single-type active sites located at interface sites in the CeO_{2-x}/Cu catalyst for CO and H_2 oxidation.

The cycling stability of CeO_{2-x}/Cu catalyst was examined by shutdown-restart test (Figure 7c). Its catalytic performance was quite stable in five-cycle test, without noticeable deterioration in CO conversion efficiency within the temperature window of 120−210 °C when comparing to the fresh catalyst CeO_{2-x}/Cu. What's more, the operation window of CeO_{2-x}/Cu catalyst is 2-fold wider than that of the typical binary oxides catalyst, for example, CeO_2/CuO and 5-fold wider than that of CeO_2/Cu reference (Figure 7d). It is concluded that the overall CO-PROX performance behavior ranks in a sequence of CeO_{2-x}/Cu ≫ CeO_2/CuO > CeO_2/Cu ≫ CeO_2 or Cu.

The effects of H_2O and CO_2 on the catalytic performance were examined and illustrated in Figures S10 and S11. As demonstrated in Figure S10, it is clear that H_2O has a negative

DOI: 10.1021/acsami.5b06302
ACS Appl. Mater. Interfaces 2015, 7, 22999−23007

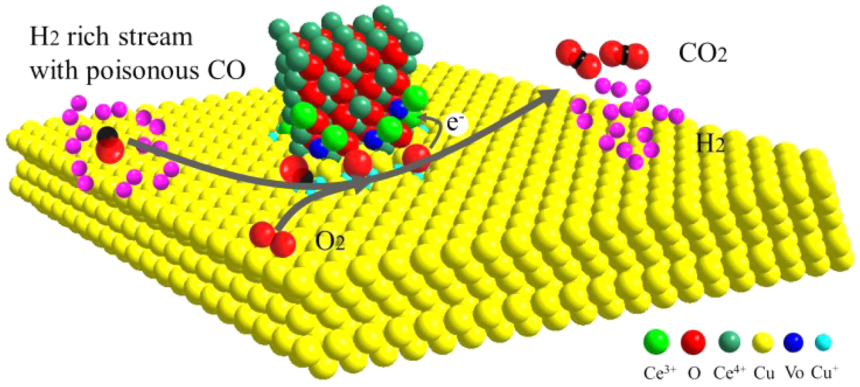

Figure 8. Schematic mechanism of CeO_{2-x}/Cu catalyst operated under CO-PROX conditions.

effect on CO conversion in the temperature range below 150 °C. Nevertheless, the conversion could still reach nearly to 100% in the temperature range from 150 to 180 °C. That is, the poisoned CO could be removed to a level below 10 ppm. Even at 210 °C, about 90% CO conversion was achieved. Comparatively, CO_2 selectivity was enhanced in the presence of water, suggesting that the side-reaction of H_2 oxidation was inhibited in the wet environment. As shown in Figure S11, CO_2 has a great influence on the catalytic activity at temperatures below 150 °C, indicating that CO oxidation was inhibited at low temperature. As the temperature increased to 150 °C or above, the influence of CO_2 was not obvious. For example, CO conversion was about 95% at 150 °C, 100% at 180 °C and about 90% at 210 °C. Similar to that in the presence of water, CO_2 selectivity was also enhanced at 15% CO_2 flowing. More importantly, the catalyst shows an excellent long-time stability at the condition that simulates the practical CO-PROX environment in the presence of H_2O and CO_2 together. As demonstrated in Figure S12, for example, 100% CO conversion could maintain as long as 105 h at 150 °C, and CO_2 selectivity was also enhanced substantially compared to the test in the dry streams. Possessing the merits of high CO conversion efficiency in a wide temperature-operation window and great stability, the current CeO_{2-x}/Cu catalyst, anchored by oxygen vacancies at interfaces, would bring about a great leap in practical usages with breakthrough in the critical issues aforementioned.

Figure 8 illustrates mechanistically how the present high efficient CeO_{2-x}/Cu catalyst works. The anchored oxygen vacancies play a bridging role in electron capture or transfer, and could drive molecule oxygen into active oxygen species. First, Cu substrate could donate electrons to the adjacent CeO_2 to form Ce^{3+}−V_O and meanwhile produce Cu^+ and reactive oxygen that are anchored at interfacial site.[17] When adsorbed onto Cu^+, CO molecules would be directly oxidized by adjacent active oxygen species.[56] Then gas-phase oxygen molecules could be quickly captured by the electron-rich oxygen vacancies and continuously produce new active species around interface.[6,58] In the meantime, the competitive molecules H_2 may dissociate on Cu^0 at noninterface sites and thus could not be oxidized due to the absence of active oxygen species nearby, which conversely favors the preferential CO oxidation.[59,60] Thus, the way that the CeO_{2-x}/Cu catalyst works could be attributed to the synergetic effect of Ce^{3+}−V_O coupled with Cu^+. In essence, the interfacial oxygen vacancies anchored offer the active oxygen species that give rise to the great performance in preferential CO oxidation, even at high temperature range. Further studies will be necessary to clarify the redox process of the preferential oxidation system.

All described above have demonstrated a chemical methodology of fixing high-concentration oxygen vacancies at interfaces of CeO_{2-x}/Cu system. In fact, for a long time, researchers struggled to find suitable materials as effective inverse catalyst with oxygen vacancies anchoring at interface sites essential for targeted preferential CO oxidation. On the basis of findings reported in this study and the fundamental chemical nature of oxides and metal, the following considerations could be highly helpful: (1) For any inverse catalysts of oxide/metal, metal support should donate electrons easily. A transition metal with d^{10} configuration is promising in this regard. (2) Oxide should have an excellent redox and oxygen storage capability. (3) For preferential CO oxidation, oxide/metal hybrid structure should be designed active for CO and O_2 simultaneously. Concerning the synthesis and microstructures of inverse catalyst, one may need to use the intermediates to control the particle size of metal support and active oxide. Moreover, the intermediates should be prepared in one-pot, which guarantees a close contact of final metal and oxide. Eventually, the intermediate of the metal support should be a loose structure, such as layered structure or porous-structures, which is convenient for the embedding process of nano-oxide.

4. CONCLUSION

A hybrid catalyst CeO_{2-x}/Cu for preferential CO oxidation in H_2-rich streams was initially synthesized through a facile chemical process. The present catalyst has shown a rather high activity, stable cycling performance, excellent long-time stability at the simulated operation environment. The temperature span is encouragingly 2−5-fold wider for reducing the poisonous CO to a level below 10 ppm, when comparing to the conventional catalysts CeO_2/CuO or CeO_2/Cu. The excellent performance of the present catalyst is beneficial from the high-concentration oxygen vacancies anchored at interfacial sites of the hybrid catalyst, which plays a mediating role in electron transfer and copper/oxygen species activation. Due to a large family of metal-oxides, it shows great potential to synthesize outstanding hybrid catalysts following the methodology reported here. The concept of anchoring high-concentration oxygen vacancies at interfaces could thus offer new perspectives for designing high-performance catalysts.

DOI: 10.1021/acsami.5b06302
ACS Appl. Mater. Interfaces 2015, 7, 22999−23007

■ ASSOCIATED CONTENT

Supporting Information

The Supporting Information is available free of charge on the ACS Publications website at DOI: 10.1021/acsami.5b06302.

XRD, DRIFTS, XPS, TPR analysis, HRTEM, and catalytic performance (PDF)

■ AUTHOR INFORMATION

Corresponding Author

* E-mail: guangshe@fjirsm.ac.cn.

Funding

This work was financially supported by the National Natural Science Foundation of China (21025104, 21271171, and 91022018).

Notes

The authors declare no competing financial interest.

■ ACKNOWLEDGMENTS

The authors are grateful to Mr. Meimei Liu, Dr. Ping Huang, and Dr. Yunhui He for their technical assistance and Dr. Minglei Zhao and Dr. Chaochao Fu for their helps in data analysis.

■ REFERENCES

(1) Liang, X.; Xu, B.; Kuang, S.; Wang, X. Multi-Functionalized Inorganic-Organic Rare Earth Hybrid Microcapsules. *Adv. Mater.* **2008**, *20*, 3739−3744.

(2) Wang, J.; Tan, H.; Yu, S.; Zhou, K. Morphological Effects of Gold Clusters on the Reactivity of Ceria Surface Oxygen. *ACS Catal.* **2015**, *5*, 2873−2881.

(3) Wang, X.; Liu, D.; Song, S.; Zhang, H. Pt@CeO_2 Multicore@Shell Self-Assembled Nanospheres: Clean Synthesis, Structure Optimization, and Catalytic Applications. *J. Am. Chem. Soc.* **2013**, *135*, 15864−15872.

(4) Zhang, J.; Li, L.; Huang, X.; Li, G. Fabrication of Ag−CeO_2 Core−Shell Nanospheres with Enhanced Catalytic Performance Due to Strengthening of the Interfacial Interactions. *J. Mater. Chem.* **2012**, *22*, 10480−10487.

(5) Esch, F.; Fabris, S.; Zhou, L.; Montini, T.; Africh, C.; Fornasiero, P.; Comelli, G.; Rosei, R. Electron Localization Determines Defect Formation on Ceria Substrates. *Science* **2005**, *309*, 752−755.

(6) Liu, X.; Zhou, K.; Wang, L.; Wang, B.; Li, Y. Oxygen Vacancy Clusters Promoting Reducibility and Activity of Ceria Nanorods. *J. Am. Chem. Soc.* **2009**, *131*, 3140−3141.

(7) Yang, F.; Graciani, J.; Evans, J.; Liu, P.; Hrbek, J.; Sanz, J. F.; Rodriguez, J. A. CO Oxidation on Inverse CeO_x/Cu (111) Catalysts: High Catalytic Activity and Ceria-Promoted Dissociation of O_2. *J. Am. Chem. Soc.* **2011**, *133*, 3444−3451.

(8) Wang, X.; Liu, D.; Li, J.; Zhen, J.; Zhang, H. Clean Synthesis of Cu_2O@CeO_2 Core@Shell Nanocubes with Highly Active Interface. *NPG Asia Mater.* **2015**, *7*, e158.

(9) Trogadas, P.; Parrondo, J.; Ramani, V. CeO_2 Surface Oxygen Vacancy Concentration Governs in Situ Free Radical Scavenging Efficacy in Polymer Electrolytes. *ACS Appl. Mater. Interfaces* **2012**, *4*, 5098−5102.

(10) Rodriguez, J. A.; Graciani, J.; Evans, J.; Park, J. B.; Yang, F.; Stacchiola, D.; Senanayake, S. D.; Ma, S.; Pérez, M.; Liu, P.; Sanz, J. F.; Hrbek, J. Water-Gas Shift Reaction on a Highly Active Inverse CeO_x/Cu (111) Catalyst: Unique Role of Ceria Nanoparticles. *Angew. Chem., Int. Ed.* **2009**, *48*, 8047−8050.

(11) Rodriguez, J. A.; Ma, S.; Liu, P.; Hrbek, J.; Evans, J.; Perez, M. Activity of CeO_x and TiO_x Nanoparticles Grown on Au (111) in the Water-Gas Shift Reaction. *Science* **2007**, *318*, 1757−1760.

(12) Grunwaldt, J. D.; Baiker, A. Gold/Titania Interfaces and Their Role in Carbon Monoxide Oxidation. *J. Phys. Chem. B* **1999**, *103*, 1002−1012.

(13) Liu, Z.-P.; Jenkins, S. J.; King, D. A. Origin and Activity of Oxidized Gold in Water-Gas-Shift Catalysis. *Phys. Rev. Lett.* **2005**, *94*, 196102.

(14) Yang, J. J.; Pickett, M. D.; Li, X. M.; Ohlberg, D. A. A.; Stewart, D. R.; Williams, R. S. Memristive Switching Mechanism for Metal/Oxide/Metal Nanodevices. *Nat. Nanotechnol.* **2008**, *3*, 429−433.

(15) Hornés, A.; Hungría, A.; Bera, P.; López Cámara, A.; Fernández-García, M.; Martínez-Arias, A.; Barrio, L.; Estrella, M.; Zhou, G.; Fonseca, J.; Hanson, J.; Rodriguez, J. Inverse CeO_2/CuO Catalyst as an Alternative to Classical Direct Configurations for Preferential Oxidation of CO in Hydrogen-Rich Stream. *J. Am. Chem. Soc.* **2010**, *132*, 34−35.

(16) Zeng, S. H.; Zhang, W.; Śliwa, M.; Su, H. Q. Comparative Study of CeO_2/CuO and CuO/CeO_2 Catalysts on Catalytic Performance for Preferential CO Oxidation. *Int. J. Hydrogen Energy* **2013**, *38*, 3597−3605.

(17) Liu, K.; Wang, A.; Zhang, T. Recent Advances in Preferential Oxidation of CO Reaction over Platinum Group Metal Catalysts. *ACS Catal.* **2012**, *2*, 1165−1178.

(18) Alayoglu, S.; Nilekar, A. U.; Mavrikakis, M.; Eichhorn, B. Ru-Pt Core-Shell Nanoparticles for Preferential Oxidation of Carbon Monoxide in Hydrogen. *Nat. Mater.* **2008**, *7*, 333−338.

(19) Song, C. Fuel Processing for Low-Temperature and High-Temperature Fuel Cells Challenges, and Opportunities for Sustainable Development in the 21st Century. *Catal. Today* **2002**, *77*, 17−49.

(20) Sharaf, O. Z.; Orhan, M. F. An Overview of Fuel Cell Technology: Fundamentals and Applications. *Renewable Sustainable Energy Rev.* **2014**, *32*, 810−853.

(21) Hernandez, J.; Gomez, S. A.; Zepeda, T. A.; Fierro-Gonzalez, J. C.; Fuentes, G. A. Insight into the Deactivation of Au/CeO_2 Catalysts Studied by in-Situ Spectroscopy During the CO-PROX Reaction. *ACS Catal.* **2015**, *5*, 4003−4012.

(22) Besenbacher, F.; Chorkendorff, I.; Clausen, B. S.; Hammer, B.; Molenbroek, A. M.; Norskov, J. K.; Stensgaard, I. Design of a Surface Alloy Catalyst for Steam Reforming. *Science* **1998**, *279*, 1913−1915.

(23) Nilekar, A. U.; Alayoglu, S.; Eichhorn, B.; Mavrikakis, M. Preferential CO Oxidation in Hydrogen: Reactivity of Core-Shell Nanoparticles. *J. Am. Chem. Soc.* **2010**, *132*, 7418−7428.

(24) Zhai, Y.; Pierre, D.; Si, R.; Deng, W.; Ferrin, P.; Nilekar, A. U.; Peng, G.; Herron, J. A.; Bell, D. C.; Saltsburg, H.; Mavrikakis, M.; Flytzani-Stephanopoulos, M. Alkali-Stabilized Pt-OH_x Species Catalyze Low-Temperature Water-Gas Shift Reactions. *Science* **2010**, *329*, 1633−1636.

(25) Huber, G. W.; Shabaker, J.; Dumesic, J. Raney Ni-Sn Catalyst for H_2 Production from Biomass-Derived Hydrocarbons. *Science* **2003**, *300*, 2075−2077.

(26) Barrio, L.; Estrella, M.; Zhou, G.; Wen, W.; Hanson, J. C.; Hungría, A. B.; Hornés, A.; Fernández-García, M.; Martínez-Arias, A.; Rodriguez, J. A. Unraveling the Active Site in Copper−Ceria Systems for the Water− Gas Shift Reaction: In Situ Characterization of an Inverse Powder CeO_{2-x}/CuO−Cu Catalyst. *J. Phys. Chem. C* **2010**, *114*, 3580−3587.

(27) Reina, T.; Papadopoulou, E.; Palma, S.; Ivanova, S.; Centeno, M.; Ioannides, T.; Odriozola, J. A. Could an Efficient WGS Catalyst Be Useful in the CO-PrOx Reaction? *Appl. Catal., B* **2014**, *150*, 554−563.

(28) Ko, E.-Y. Y.; Park, E. D.; Lee, H. C.; Lee, D.; Kim, S. Supported Pt-Co Catalysts for Selective CO Oxidation in a Hydrogen-Rich Stream. *Angew. Chem., Int. Ed.* **2007**, *46*, 734−737.

(29) Maciel, C. G.; Silva, T. d. F.; Hirooka, M. I.; Belgacem, M. N.; Assaf, J. M. Effect of Nature of Ceria Support in CuO/CeO_2 Catalyst for PROX-CO Reaction. *Fuel* **2012**, *97*, 245−252.

(30) Gamarra, D.; Belver, C.; Fernandez-García, M.; Martínez-Arias, A. Selective CO Oxidation in Excess H_2 over Copper-Ceria Catalysts: Identification of Active Entities/Species. *J. Am. Chem. Soc.* **2007**, *129*, 12064−12065.

DOI: 10.1021/acsami.5b06302
ACS Appl. Mater. Interfaces 2015, 7, 22999−23007

(31) Yen, H.; Seo, Y.; Kaliaguine, S.; Kleitz, F. Tailored Mesostructured Copper/Ceria Catalysts with Enhanced Performance for Preferential Oxidation of CO at Low Temperature. *Angew. Chem., Int. Ed.* **2012**, *51*, 12032−12035.
(32) Tada, M.; Bal, R.; Mu, X.; Coquet, R.; Namba, S.; Iwasawa, Y. Low-Temperature PrOx (Preferential Oxidation) on Novel CeO_2-Supported Cu-Cluster Catalysts under Fuel-Cell Operating Conditions. *Chem. Commun.* **2007**, 4689−4691.
(33) Moretti, E.; Lenarda, M.; Storaro, L.; Talon, A.; Frattini, R.; Polizzi, S.; Rodríguez-Castellón, E.; Jiménez-López, A. Catalytic Purification of Hydrogen Streams by PROX on Cu Supported on an Organized Mesoporous Ceria-Modified Alumina. *Appl. Catal., B* **2007**, *72*, 149−156.
(34) Cámara, A. L.; Corberán, V. C.; Barrio, L.; Zhou, G.; Si, R.; Hanson, J. C.; Monte, M.; Conesa, J. C.; Rodriguez, J. A.; Martínez-Arias, A. Improving the CO-PROX Performance of Inverse CeO_2/CuO Catalysts: Doping of the CuO Component with Zn. *J. Phys. Chem. C* **2014**, *118*, 9030−9041.
(35) Chen, C.; Wang, R.; Shen, P.; Zhao, D.; Zhang, N. Inverse CeO_2/CuO Catalysts Prepared from Heterobimetallic Metal−Organic Framework Precursor for Preferential CO Oxidation in H_2-Rich Stream. *Int. J. Hydrogen Energy* **2015**, *40*, 4830−4839.
(36) Zeng, S. H.; Zhang, L.; Jiang, N.; Gao, M. Y.; Zhao, X. Z.; Yin, Y. L.; Su, H. Q. Multi-Wall Carbon Nanotubes as Support of Copper-Cerium Composite for Preferential Oxidation of Carbon Monoxide. *J. Power Sources* **2015**, *293*, 1016−1023.
(37) Cecilia, J. A.; Arango-Diaz, A.; Rico-Perez, V.; Bueno-Lopez, A.; Rodriguez-Castellon, E. The Influence of Promoters (Zr, La, Tb, Pr) on the Catalytic Performance of CuO-CeO_2 Systems for the Preferential Oxidation of CO in the Presence of CO_2 and H_2O. *Catal. Today* **2015**, *253*, 115−125.
(38) Cecilia, J. A.; Arango-Diaz, A.; Franco, F.; Jimenez-Jimenez, J.; Storaro, L.; Moretti, E.; Rodriguez-Castellon, E. CuO-CeO_2 Supported on Montmorillonite-Derived Porous Clay Heterostructures (Pch) for Preferential CO Oxidation in H_2-Rich Stream. *Catal. Today* **2015**, *253*, 126−136.
(39) Nolan, M. Charge Transfer and Formation of Reduced Ce^{3+} Upon Adsorption of Metal Atoms at the Ceria (110) Surface. *J. Chem. Phys.* **2012**, *136*, 134703.
(40) Liu, S.; Wu, Z.; Zhang, Y.; Yao, Z.; Fan, J.; Zhang, Y.; Hu, J.; Zhang, P.; Shao, G. Strong Temperature-Dependent Crystallization, Phase Transition, Optical and Electrical Characteristics of P-Type $CuAlO_2$ Thin Films. *Phys. Chem. Chem. Phys.* **2015**, *17*, 557−562.
(41) Vayssilov, G. N.; Lykhach, Y.; Migani, A.; Staudt, T.; Petrova, G. P.; Tsud, N.; Skála, T.; Bruix, A.; Illas, F.; Prince, K. C.; et al. Support Nanostructure Boosts Oxygen Transfer to Catalytically Active Platinum Nanoparticles. *Nat. Mater.* **2011**, *10*, 310−315.
(42) Xu, B.; Yang, H.; Zhou, G.; Wang, X. Strong Metal-Support Interaction in Size-Controlled Monodisperse Palladium-Hematite Nano-Heterostructures During a Liquid-Solid Heterogeneous Catalysis. *Science China Materials* **2014**, *57*, 34−41.
(43) Liu, B. One-Dimensional Copper Hydroxide Nitrate Nanorods and Nanobelts for Radiochemical Applications. *Nanoscale* **2012**, *4*, 7194−7198.
(44) Henrist, C.; Traina, K.; Hubert, C.; Toussaint, G.; Rulmont, A.; Cloots, R. Study of the Morphology of Copper Hydroxynitrate Nanoplatelets Obtained by Controlled Double Jet Precipitation and Urea Hydrolysis. *J. Cryst. Growth* **2003**, *254*, 176−187.
(45) Ke, J.; Xiao, J.-W.; Zhu, W.; Liu, H.; Si, R.; Zhang, Y.-W.; Yan, C.-H. Dopant-Induced Modification of Active Site Structure and Surface Bonding Mode for High-Performance Nanocatalysts: CO Oxidation on Capping-Free (110)-Oriented CeO_2: Ln (Ln= La−Lu) Nanowires. *J. Am. Chem. Soc.* **2013**, *135*, 15191−15200.
(46) Behrens, M.; Studt, F.; Kasatkin, I.; Kühl, S.; Hävecker, M.; Abild-Pedersen, F.; Zander, S.; Girgsdies, F.; Kurr, P.; Kniep, B.-L. L.; Tovar, M.; Fischer, R. W.; Nørskov, J. K.; Schlögl, R. The Active Site of Methanol Synthesis over Cu/ZnO/Al_2O_3 Industrial Catalysts. *Science* **2012**, *336*, 893−897.
(47) Wu, L.; Wiesmann, H.; Moodenbaugh, A.; Klie, R.; Zhu, Y.; Welch, D.; Suenaga, M. Oxidation State and Lattice Expansion of CeO_{2-x} Nanoparticles as a Function of Particle Size. *Phys. Rev. B: Condens. Matter Mater. Phys.* **2004**, *69*, 125415.
(48) Aidhy, D. S.; Zhang, Y.; Weber, W. J. (001) $SrTiO_3$|(001) MgO Interface and Oxygen-Vacancy Stability from First-Principles Calculations. *ACS Appl. Mater. Interfaces* **2014**, *6*, 15536−15541.
(49) Lee, Y.; He, G.; Akey, A. J.; Si, R.; Flytzani-Stephanopoulos, M.; Herman, I. P. Raman Analysis of Mode Softening in Nanoparticle $CeO_{2-\delta}$ and Au- $CeO_{2-\delta}$ During CO Oxidation. *J. Am. Chem. Soc.* **2011**, *133*, 12952−12955.
(50) Deshpande, S.; Patil, S.; Kuchibhatla, S. V. N. T.; Seal, S. Size Dependency Variation in Lattice Parameter and Valency States in Nanocrystalline Cerium Oxide. *Appl. Phys. Lett.* **2005**, *87*, 133113.
(51) Bêche, E.; Charvin, P.; Perarnau, D.; Abanades, S.; Flamant, G. Ce 3d XPS Investigation of Cerium Oxides and Mixed Cerium Oxide ($Ce_xTi_yO_z$). *Surf. Interface Anal.* **2008**, *40*, 264−267.
(52) Yang, F.; Graciani, J.; Evans, J.; Liu, P.; Hrbek, J.; Sanz, J. F.; Rodriguez, J. A. CO Oxidation on Inverse CeO_x/Cu(111) Catalysts: High Catalytic Activity and Ceria-Promoted Dissociation of O_2. *J. Am. Chem. Soc.* **2011**, *133*, 3444−3451.
(53) Nilekar, A.; Alayoglu, S.; Eichhorn, B.; Mavrikakis, M. Preferential CO Oxidation in Hydrogen: Reactivity of Core-Shell Nanoparticles. *J. Am. Chem. Soc.* **2010**, *132*, 7418−7428.
(54) Carrettin, S.; Concepción, P.; Corma, A.; López Nieto, J. M.; Puntes, V. F. Nanocrystalline CeO_2 Increases the Activity of Au for CO Oxidation by Two Orders of Magnitude. *Angew. Chem., Int. Ed.* **2004**, *43*, 2538−2540.
(55) Wang, L.; Lu, G.; Yang, D.; Wang, J.; Zhu, Z.; Wang, Z.; Zhou, K. Manipulation of the Reducibility of Ceria-Supported Au Catalysts by Interface Engineering. *ChemCatChem* **2013**, *5*, 1308−1312.
(56) Shi, J. On the Synergetic Catalytic Effect in Heterogeneous Nanocomposite Catalysts. *Chem. Rev.* **2013**, *113*, 2139−2181.
(57) Huang, Y.; Wang, A.; Li, L.; Wang, X.; Su, D.; Zhang, T. Ir-in-Ceria": A Highly Selective Catalyst for Preferential CO Oxidation. *J. Catal.* **2008**, *255*, 144−152.
(58) Cui, X.; Chen, L.; Wang, Y.; Chen, H.; Zhao, W.; Li, Y.; Shi, J. Fabrication of Hierarchically Porous RuO_2−CuO/Al−ZrO_2 Composite as Highly Efficient Catalyst for Ammonia-Selective Catalytic Oxidation. *ACS Catal.* **2014**, *4*, 2195−2206.
(59) Göltl, F.; Houriez, C. l.; Guitou, M.; Chambaud, G.; Sautet, P. Importance of a Nonlocal Description of Electron−Electron Interactions in Modeling the Dissociative Adsorption of H_2 on Cu (100). *J. Phys. Chem. C* **2014**, *118*, 5374−5382.
(60) Díaz, C.; Pijper, E.; Olsen, R.; Busnengo, H.; Auerbach, D.; Kroes, G. Chemically Accurate Simulation of a Prototypical Surface Reaction: H_2 Dissociation on Cu (111). *Science* **2009**, *326*, 832−834.

DOI: 10.1021/acsami.5b06302
ACS Appl. Mater. Interfaces 2015, 7, 22999−23007